2017 American Control Conference
Sheraton Seattle Hotel
May 24–26, 2017, Seattle, USA

$\mathcal{H}_\infty$ controller design for closed-loop wake redirection

Steffen Raach[1], Jan-Willem van Wingerden[2], Sjoerd Boersma[2], David Schlipf[1], Po Wen Cheng[1]

Abstract— **The focus of control research in wind energy has shifted more and more from individual wind turbines to wind farms due to the potential efficiency improvement in the energy production. In this work, the wind farm control concept "wake redirection" is further investigated. More precisely, the concept of lidar-based closed-loop wake redirection is extended. A lidar-based wake center estimation is assumed and fed back to a controller, which steers the wake by employing the yaw actuator to a desired position. In this work, a $\mathcal{H}_\infty$ controller design approach for lidar-based closed-loop wake redirection is investigated. The controller is designed using models that are obtained from the wind farm simulation tool WFSim. First, a model identification procedure is applied to derive the controller design models. Then, a $\mathcal{H}_\infty$ controller design is conducted to obtain a controller for each identified model. The controllers are presented and the performances are analyzed. In a final step, a single controller is implemented in WFSim and closed-loop step simulations are conducted illustrating the desired behavior.**

I. Introduction

The importance of improving wind energy production is increasing as more and more countries deploy renewable energy technologies. To compete with other renewable or conventional energy sources, new control strategies are necessary to improve the power production. Lately, the focus of control applications in wind energy has shifted more and more from wind turbine control to wind farm control. The wake interactions between the wind turbines become on a wind farm level important, and should be taken into account for controller design. A wind turbine is extracting energy from the wind flow and therefore, behind a wind turbine, the wind speed is reduced with respect to the free stream velocity. Additionally, the turbulence in the wake is increased. If a second wind turbine is placed in hit a wake of a wind turbine located upwind, the wind turbine will produce less power and will be faced higher structural loads because of the increased turbulence (see, e.g., [1]).

In general, the main control goals for wind farm control are equal to wind turbine control: 1) increasing power production, and 2) decreasing structural loads. Since wind turbines interacting through their flow, a wind farm is highly complex and distributed. Currently, there are two main concepts for wind farm control: 1) axial induction control, and 2) wake redirection control. This paper is focusing on the latter. However, a brief overview of the first will be given now.

Axial induction control aims to achieve a better performance in a sense of the two control goals by intelligently curtailing the wind turbines. Different results have been achieved using this approach. Results obtained with the high-fidelity computational fluid dynamics (CFD) simulation tool SOWFA (Simulator fOr Wind Farm Applications, see [2]) illustrates that performance increase seems hardly achievable, see [3]. Consider [4] for a more precisely summary and current research questions on axial induction wind farm control.

The idea of wake redirection is to deflect the wake and avoid wake overlap with a downwind turbine. This can be done by cyclic blade pitching or by yawing the wind turbine, see [5], [6] respectively. In [7], wake redirection was investigated to increase the total power output of a wind farm by using game theory and a steady-state parametric wake model to obtain optimized yaw angles. The optimized yaw angles are then applied to the wind farm and a higher total power output was observed. In [5], wake redirection was studied in the high fidelity simulation tool SOWFA by applying offsets to the yaw angle and studying the steady state results of wake redirection. For more information on wind farm control and modelling, we refer to [4].

Altogether, the approach of wake redirection looks very promising for improving the power output of a wind farm, although the form in which it has been applied so far does contain drawbacks: 1) Applying optimized yaw angles in a feed-forward approach does not guarantee that the wake is going to the desired direction - thus, the quality of the model, which is used to compute the yaw angles, highly influences the control performance. 2) There is no observation of whether the wake is being redirected correctly.

A nacelle-based lidar can provide wake position information to a controller, see [8]. Thus, having a feedback of wake information would make the approach more robust in case of disturbances or model uncertainties. First simulation results of a wind farm with six wind turbines have shown an improvement of the power output compared to the feed-forward approach, see [9]. In the following subsection, the concept of lidar-based close-loop wake redirection is described.

A. Lidar-based closed-loop wake redirection

Using lidar measurements behind the wind turbine gives an insight into the wake flow. Estimation techniques are used to obtain the wake center position and provide it to a controller. Compared to previous approaches in wind farm control, this concept enables a direct feedback of flow information and therefore, a direct control of them. In [9], a first controller was introduced that directly controls the

[1] are with Stuttgart Wind Energy (SWE), University of Stuttgart, Stuttgart, Germany
[2] are with Delft University of Technology, Delft, Netherlands
Point of contact: raach@ifb.uni-stuttgart.de

978-1-5090-5992-8/$31.00 ©2017 AACC

wake center and thereby improves the total power output of the wind farm. The main concept is sketched in Fig. 1.

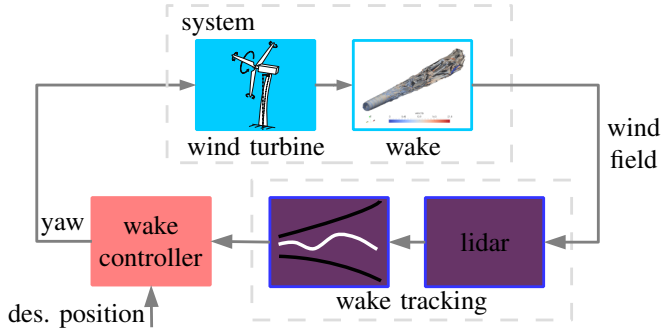

Fig. 1: The general concept of lidar-based closed-loop wake redirection: The main idea is to use lidar measurements and a wake tracking technique to estimate the wake center position and feedback this information to a controller. The controller redirects the wake center position by yawing the wind turbine such that the wake center moves to the desired position.

B. Motivation and objectives

This paper is motivated by the controller approach presented in [9]. There, an internal model controller approach for wake steering was investigated. In [9], the controller design model was developed by simplifying the simulation model SimWindFarm [10]. It was then used in an internal model controller to predict the output of the real system. In contrast to [9], in this work, a model identification is performed to obtain a model for controller design. Further, a $\mathcal{H}_\infty$ controller design synthesis is used to design a controller, which gives the possibility of directly defining the controller performance in the frequency domain. The main contributions of this paper are:

1) a parametric model identification from lidar-based wake redirection,
2) a $\mathcal{H}_\infty$ controller design for lidar-based wake redirection, and
3) a simulation study in a medium-fidelity model with the obtained controller.

The paper is structured as follows: first, the simulation model is shortly reviewed and summarized. Second, the model identification is presented. Then, the controller design is shown in Sec. IV. In Sec. V, simulation results are discussed and finally, in Sec. VI conclusions are given.

II. Simulation Model

For this work, the two-dimensional Navier-Stokes simulation model for wind farm simulations (WFSim) [11] is used. In the following, the simulation model is briefly described and the wake center estimation approach is presented.

A. Wind farm simulation model WFSim

WFSim is a two-dimensional flow model that can compute flow vectors for a given wind farm topology. The solver is based on the unsteady 2D Navier-Stokes equations:

$$\frac{\partial \mathbf{u}}{\partial t} + (\mathbf{u}\cdot\nabla)\mathbf{u} + \frac{1}{\rho}\nabla p - \frac{\mu}{\rho}\nabla^2\mathbf{u} = \mathbf{f},$$
$$\mathbf{u}\cdot\nabla = 0, \tag{1}$$

$$\text{with} \quad \nabla = [\tfrac{\partial}{\partial x} \ \tfrac{\partial}{\partial y}]^T \quad \text{and} \ \nabla^2 = \tfrac{\partial^2}{\partial x^2} + \tfrac{\partial^2}{\partial y^2}. \tag{2}$$

The term $\mathbf{f}$ represents the turbines while $\mathbf{u} = [u\ v]^T$ and p represent the flow velocities and pressure, respectively. The air density ρ and the viscosity μ are considered to be constant. Under the boundary conditions and the forcing terms defined later, no analytic solution of the equations exist, yet. Hence, the governing equations are resolved numerically using a spatial and temporal discretization scheme. In WFSim, the state variables u_k, v_k and p_k at time step k are arranged according the grid points, e.g.,

$$u_k = \left[u_{3,2}\dots u_{3,N_{y-1}} \dots\dots u_{N_{x-1},N_{y-1}}\right]. \tag{3}$$

The constants N_x and N_y are the number of grid points in the x- and y-direction, respectively. The finite volume and implicit method are applied resulting in the following set of nonlinear algebraic difference equations:

$$\underbrace{\begin{pmatrix} A_x(u_k,v_k) & 0 & B_1 \\ 0 & A_y(u_k,v_k) & B_2 \\ B_1^T & B_2^T & 0 \end{pmatrix}}_{A(x_k)\in\mathbb{R}^{m\times m}} \underbrace{\begin{pmatrix} u_{k+1} \\ v_{k+1} \\ p_{k+1} \end{pmatrix}}_{x_{k+1}} = \underbrace{\begin{pmatrix} b_1(u_k,v_k)+S_k^x(u_k,v_k) \\ b_2(u_k,v_k)+S_k^y(u_k,v_k) \\ b_3 \end{pmatrix}}_{b(x_k)\in\mathbb{R}^{m\times 1}}, \tag{4}$$

with $m = n_u + n_v + n_p$ and $u_k \in \mathbb{R}^{n_u}, v_k \in \mathbb{R}^{n_v}, p_k \in \mathbb{R}^{n_p}$ the velocity vectors in the x-direction, y-direction and the pressure vector at time k, respectively. Each component of u_k, v_k and p_k represents, at time k, a velocity and pressure, respectively, at a point in the field defined by the subscript. Computational cost for solving this set of equations is kept low by exploiting sparsity and by applying the reverse Cuthill-McKee algorithm. The terms $b_1(u_k,v_k)$, $b_2(u_k,v_k)$ and b_3 represent the boundary conditions and the terms $S_k^x(u_k,v_k)$ and $S_k^y(u_k,v_k)$ the turbines. Both will be described next.

1) Boundary conditions: For the u and v velocity, first order conditions are prescribed on one side of the grid related to the ambient inflow defined by u_b and v_b. Zero stress boundary conditions are imposed on the other boundaries. For the initial conditions, all u and v velocity components in the field are defined as u_b and v_b respectively, the boundary velocity components. The initial pressure field is set to zero.

2) Turbine modeling: According to momentum theory, the following force term is defined:

$$S_k = C_T(a)\frac{1}{2}\rho A_r U_\infty^2, \tag{5}$$

with thrust coefficient $C_T(a)$ depending on the axial induction factor a, rotor upwind velocity U_∞, and rotor swept area A_r. The following expression for $C_T(a)$ is proposed in [12] and used in WFSim:

$$C_T(a) = \begin{cases} 4aF(1-a), & \text{if } 0 \le a \le 0.4 \\ \left(\frac{8}{9} + \frac{36F-40}{9}a + \frac{50-36F}{9}a^2\right) & \text{if } 0.4 < a < 1 \end{cases} \tag{6}$$

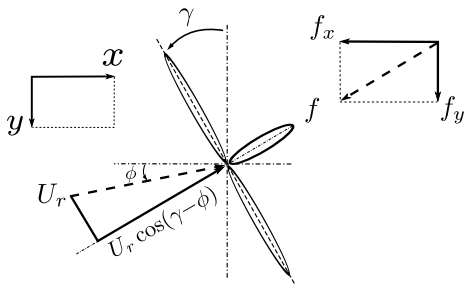

Fig. 2: Schematic representation of a turbine with yaw angle γ, wind direction angle at the rotor ϕ and rotor velocity U_r. Figure taken and adapted from [13].

The Glauert correction factor F is set to 1.75. Since U_∞ is difficult to measure in a wind farm, it is helpful to write the force in terms of the flow velocity at the rotor. The following relations are defined:

$$\beta = \frac{a}{1-a}, \quad U_\infty = \frac{U_r\cos(\gamma-\phi)}{1-a}, \quad U_r = \sqrt{u_r^2+v_r^2}, \quad (7)$$

with U_r the flow velocity vector at the rotor with direction defined by the wind direction angle ϕ and the yaw angle γ of the turbine (see Fig. 2). Substituting these relations in Eq. (5) yields the force expression S_k:

$$S_k = \frac{1}{2}\rho A_r C_T(\beta)\left[U_r\cos(\gamma-\phi)(\beta+1)\right]^2. \quad (8)$$

The forces in the x- and y-direction are now defined as:

$$S_k^x(u_k,v_k) = -S_k\cos(\gamma), \qquad S_k^y(u_k,v_k) = S_k\sin(\gamma). \quad (9)$$

B. Wake tracking in WFSim

For the purpose of determining the wake center position, a simple wake tracking algorithm was used to obtain a wake center estimation in WFSim. The algorithm is inspired by computing the area center point. At the measurement distance the velocity profile is analyzed. In the profile the first two points below 75% of the free flow wind speed U_∞ from each side of the wake deficit are taken. With the information of those points, the center point between them is computed and used as an estimation of the wake center. As mentioned, this method is very simple, however, an applicable wake tracking approach using lidar measurements is presented in [8] and will be improved within ongoing lidar wake measurements.

III. Model for Controller Design

In the following, a model identification is performed. This is necessary because linear controller design models are required for the $\mathcal{H}_\infty$ controller synthesis used in this paper.

A. Identification setup

A feasible way to determine the system dynamics is to analyze step responses of the system. A step on the input is applied and the output behavior is recorded. These signals can then be used in a system identification process to obtain a model. Here, several step simulations are conducted. The steady state from the input is removed for the model identification process. In this paper, we conduct five step simulations in which yaw actions from 0 deg to 25 deg are applied.

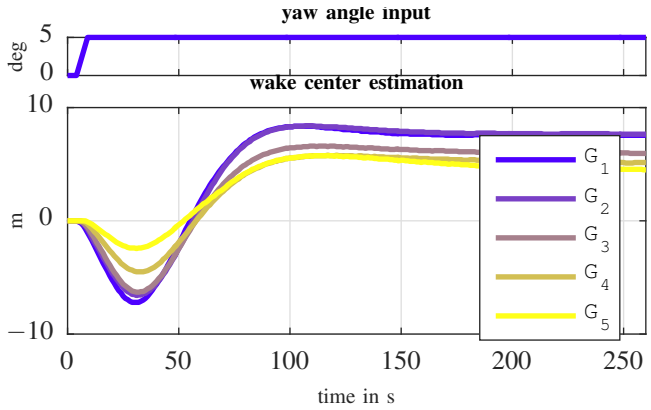

Fig. 3: Step responses of five degree steps in the yaw actuator. The steady state is subtracted for the identification and for comparing the dynamic behavior.

B. Model assumptions for identification

A model identification is performed assuming a fixed structure. The recorded input (yaw angle) and the recorded output (estimated wake center), are used in the Model Identification Toolbox of Matlab to obtain a transfer function. For more information on model identification see [14]. The model identification is performed by predefining the number of poles and zeros. An inverse output response was observed in step simulations (see Fig. 3). However, the source of this phenomenon or its existence in reality is not clear yet. High-fidelity simulations in SOWFA, however, show similar behavior. It may result from the drop in the pressure field and the very simple wake center estimation technique used in this work.

C. Model identification

In this subsection, model identification is conducted for five step responses. For the identification process, the steady states of the input and the output are removed and $n_Z = 1$ zero, and $n_P = 4$ poles are assumed for each model identification. In Fig. 3, we show the 5 deg step responses from 0 deg to 25 deg. For all plots, the color order is the same, starting from blue (step at 0 deg) to yellow (step at 20 deg). For each step response a model is identified. This yield a set of models of the form

$$G_i(s) = K_i\frac{z_{i1}s+1}{(p_{i1}s+1)(p_{i2}s+1)(p_{i3}s+1)(p_{i4}s+1)} \quad (10)$$

with p_{ij} the poles, z_{ij} the zeros, and K_i the static gain of the identified model G_i. They differ in the static gain K_i and the location of the zeros and the poles. The bode plots of all identified models are shown in Fig 4. All identified models have a normalized root mean squared error above 92 %.

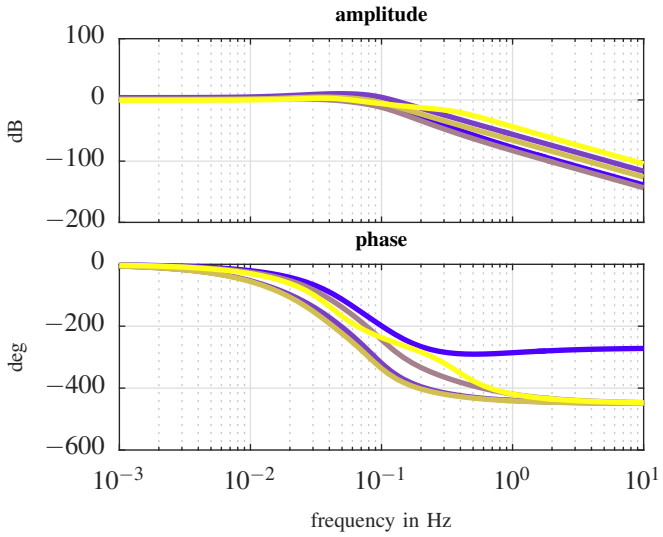

Fig. 4: Bode plots of all identified models. Starting from 0 deg yaw angle (blue) to 30 deg yaw angle (yellow).

IV. Controller design

In the following the controller design is presented. First, the $\mathcal{H}_\infty$ controller design synthesis is briefly described and then for each identified model performed.

A. Generalized plant

$\mathcal{H}_\infty$ controller synthesis makes use of the general control configuration, shown in Fig. 5, where P is the generalized plant and K the generalized controller. The idea of formulating a general control problem is to minimize the $\mathcal{H}_\infty$ norm of the transfer function from input w to performance output z, see [15]. The controller design problem is then to find a controller K that minimizes the norm. Here, w represents a disturbance entering the output ($w=-d_y$) or a reference command ($w=r$), see [15]. The general plant further provides different weighted performance measures as outputs z_1 to z_3: the sensitivity, the complementary sensitivity, and the controller sensitivity, respectively.

The generalized plant is typically used to design $\mathcal{H}_2$ or $\mathcal{H}_\infty$ controllers. The advantages of $\mathcal{H}_\infty$ controller design is mainly the ability of shaping closed-loop transfer functions and setting stability and robustness margins. Further, the controller design synthesis is a more straight forward approach compared to the work done in [9]. A final benefit is the ability to easily extend the approach to a robust controller design, which will be done in the future.

B. $\mathcal{H}_\infty$ controller design synthesis

The $\mathcal{H}_\infty$ controller synthesis considers three criteria to design and evaluate the performance of the controller. The sensitivity S, the complementary sensitivity T and the controller sensitivity U which are defined as

$$S=\frac{1}{1+GK},\qquad T=\frac{GK}{1+GK},\qquad U=\frac{K}{1+GK}. \tag{11}$$

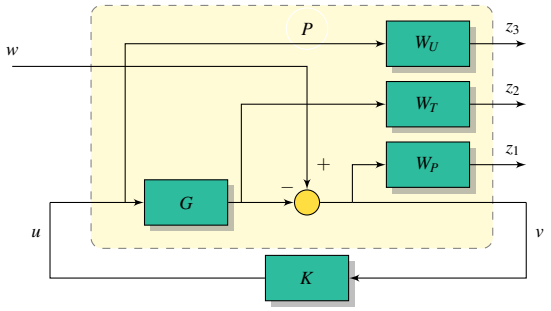

Fig. 5: Generalized plant P with performance signals z_1, z_2, and z_3 and input w. Furthermore, we have the identified model G, the performance weights W_P, W_U and W_T and controller K with control signal u, the yaw angle.

S gives the transfer function from the disturbance to the system output, T is the transfer function from the reference to the output and is further the complement of S, and $-U$ is the transfer function from the disturbance to the control signal.

For the closed-loop, a good disturbance rejection is desired and therefore, S should be small for low frequencies. Further, the control effort should be limited by having a roll-off in T after the bandwidth. In [9], a controller bandwidth of $\omega_{CL}=\frac{1}{2\tau}$ was used with the delay time τ. The delay occurs because of the flow propagation to the measurement location of the lidar. Here, the maximum controller bandwidth is given by the zero in the model. Having a real positive zero, the maximum controller bandwidth is limited to $\omega_{\mathrm{CL}}=\frac{z}{2}$, which is the frequency at which the frequency asymptote of the magnitude of the inverse plant transfer function crosses 1, (for more information, see [15]).

$W_P(s)$ is chosen to get a slope of 20 dB/dec in $|S|$ for the low frequency region as follows

$$W_P(s)=\frac{s/M+w_B}{s+Aw_B} \tag{12}$$

with the desired closed-loop bandwidth w_B, A the desired disturbance attenuation inside the bandwidth, and M the desired bound on $\|S\|_\infty$, see [15]. The complementary sensitivity is neglected by setting $W_T(s)=0$ and the controller sensitivity is penalized at high frequencies by

$$W_U(s)=1250\frac{s^2+\sqrt{2}\omega s+\omega^2}{s^2+50\sqrt{2}\omega s+(50\omega)^2} \tag{13}$$

with $\omega=0.01$. As mentioned above, the main benefits of $\mathcal{H}_\infty$ controller design synthesis is the ability to shape closed-loop frequency responses. The controller is designed such that the weighted $\mathcal{H}_\infty$ norm of transfer functions from w to z_1, z_2, and z_3 is minimized. The controller is obtained though minimizing the following mixed-sensitivity problem with respect to the controller K

$$\min_K \left\| \begin{matrix} W_PS \\ W_TT \\ W_UU \end{matrix} \right\|_\infty = \min_K \left\| \begin{matrix} W_P(1+GK)^{-1} \\ W_TGK(1+GK)^{-1} \\ W_UK(1+GK)^{-1} \end{matrix} \right\|_\infty, \tag{14}$$

with the weights $W_P(s)$, $W_T(s)$, and $W_U(s)$, respectively.

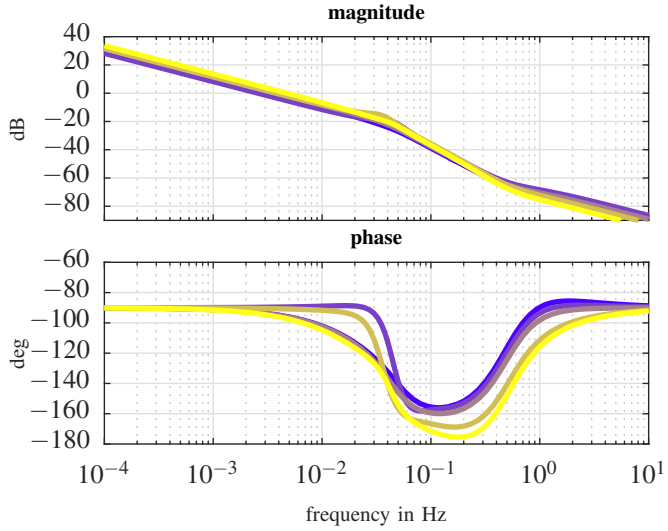

Fig. 6: The resulting controller from the $\mathcal{H}_\infty$ controller design for all plant models G_1 to G_5. Colors see Fig. 3

C. Nominal controller analysis

Having designed a controller for each identified model, first, the controller is analyzed. Fig. 6 shows the bode analysis of the designed controllers. Further, closed-loop performances are evaluated in Fig. 7: the disturbance sensitivity, the controller sensitivity and the complementary sensitivity. All controllers behave well and achieve the desired performance goals which were set in the $\mathcal{H}_\infty$ controller synthesis and shown in black in the plots.

V. Results

As a final step, the controller is implemented in WFSim to perform closed-loop wake steering. First, a single controller is chosen to perform in the whole operation region. Second, closed-loop step simulations are conducted within WFSim to evaluate the functionality and performance of the controller.

For demonstrating wake steering within WFSim, a single controller is chosen. Because of the nonlinearity of the real system, the identified models differ which can be easily seen in the bode plots in Fig. 4. Subsequently, an analysis for each controller is carried out to evaluate its performance with all identified models. A controller is then chosen which satisfies the desired margins best for all models. The results of the analysis of the chosen controller is shown in Fig. 9. Compared to the controller evaluation in Fig. 7, where the nominal performance of each closed-loop is analyzed, we still see satisfying performance. In the sensitivity, however, for some models a violation of the desired boundary for low frequencies is observed. This limitation can be overcome by a robust controller design in which model uncertainty is directly considered.

A simulation is conducted in which the wake center is estimated 1.5 times the rotor diameter downwind of the wind turbine. The desired wake center position is first set to 20 m and after 2000 s the desired wake center position is changed

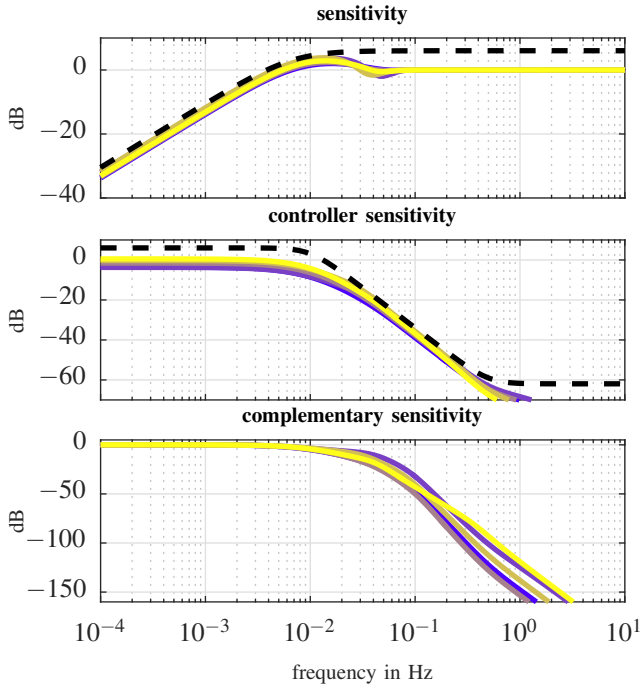

Fig. 7: Performance evaluation of the controller design: disturbance sensitivity, controller sensitivity, and complementary sensitivity. The desired performance boundaries are shown in black.

to −15 m. Fig. 8 shows flow snapshots of the simulation and time series of the wake center, the desired values, and the yaw angle of the wind turbine. The controller nicely steers the wake to the desired position and stabilizes it.

VI. Conclusion

In this work, a $\mathcal{H}_\infty$ controller design for closed-loop wake redirection in WFSim was presented. First, a model identification has been performed to obtain controller design models. Second, for each model, a $\mathcal{H}_\infty$ controller has been designed in a mixed-sensitivity approach. A single controller was then chosen for all models by evaluating their performances. Third, closed-loop simulation were conducted in which the wake was redirected to desired positions.

Altogether, this approach follows the first idea presented in [9], but uses a parametric model identification and the benefits of $\mathcal{H}_\infty$ controller design synthesis. It offers the possibility to directly define the bandwidth and the performance while keeping the benefits of closed-loop wake redirection which are: 1) a higher energy output of the wind farm, and 2) a more robust disturbance rejection and control performance.

As a next step, the approach will be implemented in a high fidelity simulation environment together with a more sophisticated lidar wake estimation approach like presented in [8]. Further, uncertainty will be included in the models to account for model mismatches. The uncertain model can then be used to design robust controllers using the same mixed-sensitivity framework.

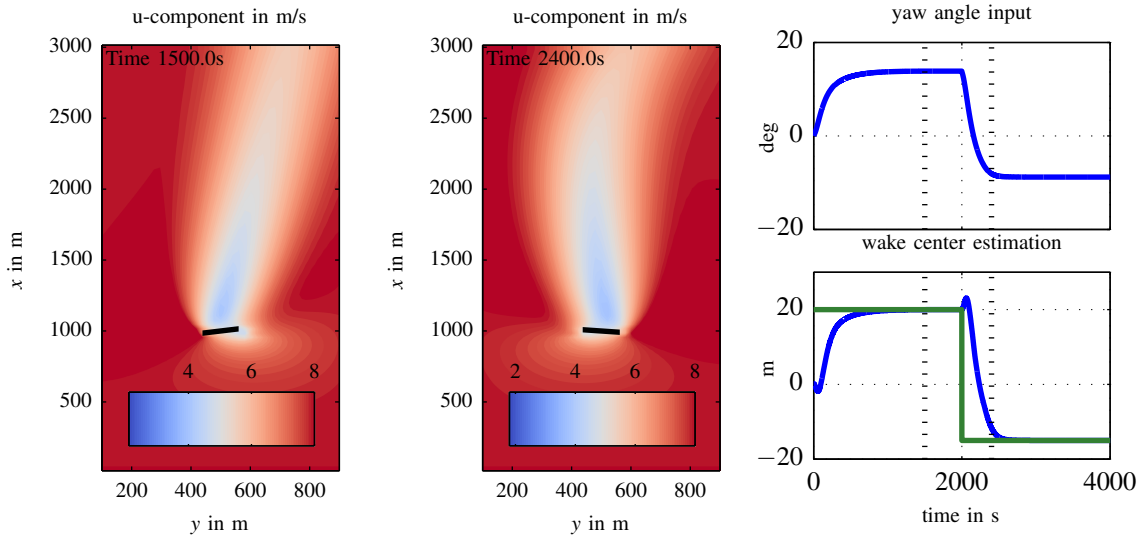

Fig. 8: Simulation results of the closed-loop simulations in WFSim. The flow snapshots are from 1500 s and from 2400 s, which is also indicated in the time series results (dotted lines). The time series shows the yaw angle and the estimated wake center. The desired wake center set points are shown in green.

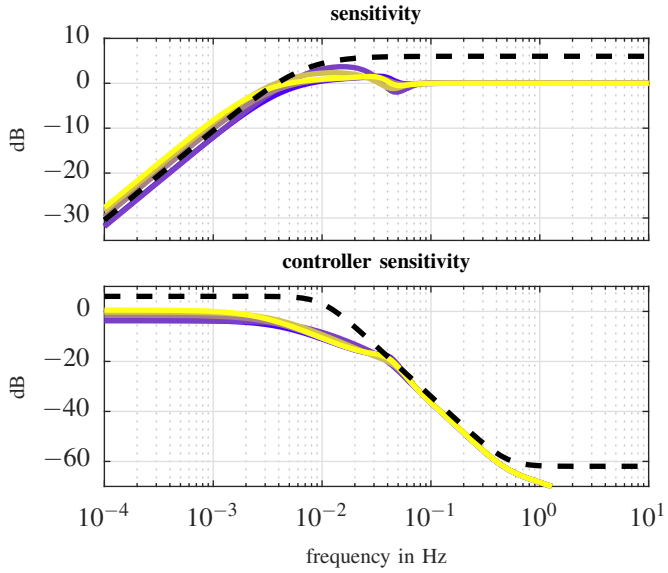

Fig. 9: Performance analysis for the chosen controller with all plants G_1 to G_5. Colors see Fig. 3.

ACKNOWLEDGMENTS

The authors would like to specially thank Paul Fleming and Andy Scholbrock of the National Renewable Energy Laboratory for the fruitful discussions and their hospitality. Further, the CL-Windcon project is acknowledged. This project has received funding from the European Union's Horizon 2020 research and innovation programme under grant agreement No 727477.

REFERENCES

[1] F. Borisade, B. Luhmann, S. Raach, and P. W. Cheng, "Shadow Effects in an Offshore Wind Farm - Potential of Vortex Methods for Wake Modelling," in *Proceedings of the DEWEK*, 2015.

[2] M. Churchfield, S. Lee, and P. Moriarty, "Overview of the Simulator for Offshore Wind Farm Application SOWFA," 2012.

[3] J. Annoni, P. Gebraad, A. Scholbrock, P. Fleming, and J.-W. van Wingerden, "Analysis of axial-induction-based wind plant control using an engineering and a high-order wind plant model," *Wind Energy*, vol. 19, no. 6, pp. 1135–1150, 2016.

[4] S. Boersma, B. Doekemeijer, P. Gebraad, J. Fleming, P.and Annoni, A. Scholbrock, J. Frederik, and J.-W. van Wingerden, "A tutorial on control-oriented modeling and control of wind farms," in *Proceedings of the American Control Conference (ACC)*, 2017.

[5] P. Fleming, P. Gebraad, S. Lee, J.-W. van Wingerden, K. Johnson, M. Churchfield, J. Michalakes, P. Spalart, and P. Moriarty, "Evaluating techniques for redirecting turbine wakes using SOWFA," *Renewable Energy*, vol. 70, pp. 211–218, 2014.

[6] ——, "Simulation comparison of wake mitigation control strategies for a two-turbine case," *Wind Energy*, vol. 18, no. 12, pp. 2135–2143, 2015.

[7] P. Gebraad, F. Teeuwisse, J.-W. van Wingerden, P. Fleming, S. Ruben, J. Marden, and L. Pao, "Wind plant power optimization through yaw control using a parametric model for wake effectsa cfd simulation study," *Wind Energy*, vol. 19, no. 1, pp. 95–114, 2016.

[8] S. Raach, D. Schlipf, and P. W. Cheng, "Lidar-based wake tracking for closed-loop wind farm control," in *Journal of Physik: Conference Series, The Science of Making Torque from Wind*, 2016.

[9] S. Raach, D. Schlipf, F. Borisade, and P. W. Cheng, "Wake redirecting using feedback control to improve the power output of wind farms," in *Proceedings of the American Control Conference (ACC)*, 2016.

[10] J. D. Grunnet, M. Soltani, T. Knudsen, M. Kragelund, and T. Bak, "Aeolus Toolbox for Dynamic Wind Farm Model, Simulation and Control," in *Proceedings of the European Wind Energy Conference*, 2010.

[11] S. Boersma, M. Vali, M. Kühn, and J.-W. van Wingerden, "Quasi linear parameter varying modeling for wind farm control using the 2D Navier-Stokes equations," in *Proceedings of the American Control Conference (ACC)*. IEEE, 2016, pp. 4409–4414.

[12] L. Marshall and J. Buhl, "A new empirical relationship between thrust coefficient and induction factor for the turbulent windmill state," National Renewable Energy Laboratory, Tech. Rep., 2005.

[13] Á. Jiménez, A. Crespo, and E. Migoya, "Application of a LES technique to characterize the wake deflection of a wind turbine in yaw," *Wind Energy*, vol. 13, no. 6, pp. 559–572, 2010.

[14] L. Ljung, Ed., *System Identification (2Nd Ed.): Theory for the User*. Upper Saddle River, NJ, USA: Prentice Hall PTR, 1999.

[15] S. Skogestad and I. Postlethwaite, *Multivariable Feedback Control: Analysis and Design*. John Wiley & Sons, 2005.